Taylor & Francis
Taylor & Francis Group

Numerical Heat Transfer, Part A: Applications
An International Journal of Computation and Methodology

ISSN: 1040-7782 (Print) 1521-0634 (Online) Journal homepage: http://www.tandfonline.com/loi/unht20

Coupled lattice Boltzmann finite volume method for conjugate heat transfer in porous media

D. Chiappini, A. Festuccia & G. Bella

To cite this article: D. Chiappini, A. Festuccia & G. Bella (2018) Coupled lattice Boltzmann finite volume method for conjugate heat transfer in porous media, Numerical Heat Transfer, Part A: Applications, 73:5, 291-306, DOI: 10.1080/10407782.2018.1444868

To link to this article: https://doi.org/10.1080/10407782.2018.1444868

Published online: 14 Mar 2018.

NUMERICAL HEAT TRANSFER, PART A
2018, VOL. 73, NO. 5, 291–306
https://doi.org/10.1080/10407782.2018.1444868

Taylor & Francis
Taylor & Francis Group

Coupled lattice Boltzmann finite volume method for conjugate heat transfer in porous media

D. Chiappini[a], A. Festuccia[b], and G. Bella[b]

[a]Department of Engineering, University of Rome 'Niccoló Cusano', Rome, Italy; [b]Department of Management Engineering, University of Rome 'Tor Vergata', Rome, Italy

ABSTRACT

This work presents a coupled lattice Boltzmann finite volume method for dealing with conjugate heat transfer problems. Lattice Boltzmann scheme is used for fluid-dynamics, while high-order finite volume method is implemented for temperature reconstruction. After a first validation with literature test cases, the method is applied to a heat exchanger with an insert made of porous medium, representative of an open-cell metal foam, innovative material largely used for its thermomechanical properties. This allows maximizing heat exchange processes with advantages in terms of efficiencies. Thus, the coupled method allows dealing with complex boundaries in multiphysics problems.

ARTICLE HISTORY
Received 11 November 2017
Accepted 18 February 2018

1. Introduction

During last decades, an always increasing attention has been addressed toward numerical simulations of complex flows and multiphysics problems, which involve the contemporary presence of two different physical phenomena. The engineering problems which belong to multiphysics are ubiquitous and spread over a large number of applications. One can think, for example, to heat exchangers where the contemporary solution of both the fluid-dynamics and the thermal fields is required. A class of innovative materials, the open-cell metal foams, which are gaining a primary role in engineering applications both for industrial or electronic devices [1, 2], is striving the development of reliable and easy-to-manage tools for multiphysics simulations. These materials present attractive characteristics both in terms of lightness and of equivalent thermal properties, thus a correct modeling of involved phenomena is mandatory. In this scenario, the possibility of coupling fluid-dynamics solver, based on lattice Boltzmann method (LBM), with a thermal one, based on finite volume method (FVM), is going to be presented. In the recent past, the lattice Boltzmann method has been extensively used for the solution of complex flows and complex geometries due to its intrinsic simplicity in implementation [3–10] and it has been deeply used for a lot of applications involving multiphase flows [11–13], non-Newtonian fluids [14, 15], etc. Thus, flow through porous media is a modeling field where LBM is an alternative to traditional numerical methods, as already demonstrated by recent advances [9, 16, 17]. Obviously, different approaches can be used to recover the physical behaviour of porous media through numerical simulations, here a random packed sphere approach [18] is used to match the general macroscopic properties of porous media, such as porosity and pores per inch distribution. Nevertheless, in its standard definition, LBM is not allowing to recover energy equation for solving thermal field. For this reason many models, which use different LBM stencils have been developed with the aim of solving the energy equation, [19–25]. In general terms, energy equation may be recovered an additional population, using the same LB stencil, which allows tracing temperature as a passive scalar

CONTACT D. Chiappini daniele.chiappini@unicusano.it University of Rome 'Niccoló Cusano', Via don Carlo Gnocchi 3, Rome 00166, Italy.
Color versions of one or more of the figures in the article can be found online at www.tandfonline.com/unht.

Nomenclature

C	specific heat
dt	energy equation time-step
$\mathbf{e}$	lattice Boltzmann local velocity
f	lattice Boltzmann population
$\mathbf{F}$	force vector
F	force component in lattice Boltzmann stencil
$\mathbf{g}$	gravitational acceleration
h	channel height
L	characteristic length
n	direction normal to surface
N_{pop}	number of stencil directions
Nu	Nusselt number
Pr	Prandtl number
Ra	Rayleigh number
Re	Reynolds number
Q	heat exchanged
$\dot{Q}$	heat flux
t	time
T	temperature
$\widetilde{T}$	non-dimensional temperature
$\overline{T}$	mean temperature
$\mathbf{u}$	fluid velocity vector
$\bar{u}$	mean horizontal velocity
u, v	velocity components
U_C	characteristic velocity
$\mathbf{X}$	position vector
x, y	spatial coordinates
$\bar{y}$	non-dimensional coordinate
w	lattice Boltzmann weight

Greek symbols

α	lattice Boltzmann direction
β	thermal expansion coefficient
δ	metal layer height
Δx	grid spacing
ΔT	hot/Cold temperature difference
ϵ	metal foam porosity
κ	thermal conductivity
ν	lattice Boltzmann kinematic viscosity
ρ	density
τ	lattice Boltzmann relaxation time
χ	thermal diffusivity

Subscripts

0	reference property
1, 2, 3, 4	heat exchanger sections
ave	average value
C	cold temperature
flu	fluid property
H	hot temperature
i, j	cartesian directions
max	maximum value
sol	solid property;
wall	wall property

Superscripts

BW	backward differencing
eq	equilibrium distribution function
FW	forward differencing
t	time-step

[19–33], or by FVM applied to the same grid of LB [34]. Synthetically, at every time step, both fluid-dynamics and energy equations are solved in a sort of fractional step: first fluid-dynamic field through LBM is solved to recover macroscopic variables such as pressure and velocity, and after, the energy equation with one of the proposed models is evaluated. The focus of this paper is addressed to conjugate heat transfer (CHT), [35–40] which is a ubiquitous phenomenon in a large number of engineering applications, such as heat exchangers. For this application, LBM for fluid-dynamic simulations seems to be a suitable approach due to its intrinsic simplicity in dealing with complex boundaries, while FVM is used to recover the energy equation both for solid and fluid phases. More precisely, CHT presents some critical aspects which have to be handled with care. In fact, as per its definition, it implies the interface between two different materials, here fluid and solid, and it has to fulfil two physical constraints. The first one is the temperature continuity at the interface, while the second is the normal flux continuity, [41, 42]. In this work, after model validation with some literature test cases, a counterflow heat exchanger with porous media insert, installed to improve heat transfer mechanism, is analyzed under different operating conditions. The work is organized in the following way: in Section 2, the lattice Boltzmann model for fluid dynamic is briefly presented; in Section 3, the FVM for energy equation is presented; in Section 4, the test cases used for model validation are briefly reported; finally, in Section 5, the heat exchange in a counterflow heat exchanger with porous media is analyzed; in Section 6, conclusions and future developments are presented.

2. Lattice Boltzmann for fluid-dynamics

Boltzmann equation describes statistical behaviour of a fluid system far from thermodynamic equilibrium. Lattice Boltzmann models simplify Boltzmann's description by reducing the number

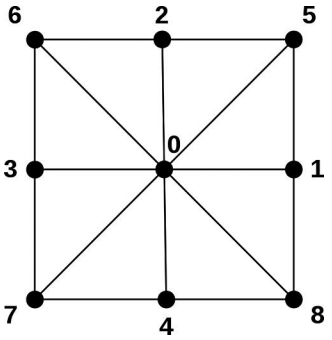

Figure 1. Schematic representation of a D_2Q_9 stencil.

of degrees of freedom of the particles. Streaming and collision define the whole dynamics of the particles. The scheme adopted in this work is D_2Q_9 which has a stencil like the one reported in Figure 1 [3–5, 43].

BGK approximation introduces a single relaxation time τ_f to greatly simplify the collision operator. It also defines the transport coefficient (viscosity for velocity and thermal diffusivity for temperature):

$$\nu = \frac{1}{3}\left(\tau_f - \frac{1}{2}\right) \tag{1}$$

Dynamics of particles is governed by streaming, collision, and forcing steps.

$$f_\alpha(\mathbf{x}+\mathbf{e}_\alpha, t+1) - f_\alpha(\mathbf{x}, t) = -\frac{1}{\tau_f}\left[f_\alpha(\mathbf{x}, t) - f_\alpha^{eq}(\mathbf{x}, t)\right] + \left(1 - \frac{1}{2\tau_f}\right)F_\alpha(\mathbf{x}, t) \quad \alpha = 0 \ldots 8 \tag{2}$$

w_α are the weighting coefficient and, for the D_2Q_9 scheme, are 4/9 ($\alpha = 0$), 1/9 ($\alpha = 1, 2, 3, 4$), and 1/36 ($\alpha = 5, 6, 7, 8$); e_α is the unitary stencil velocity. Finally, f_α^{eq} is the local equilibrium value for the population along α direction, defined as follows:

$$f_\alpha^{eq}(\mathbf{x}, t) = w_\alpha \rho(\mathbf{x}, t)\left\{1 + 3[\mathbf{e}_\alpha \cdot \mathbf{u}(\mathbf{x}, t)] + \frac{9}{2}[\mathbf{e}_\alpha \cdot \mathbf{u}(\mathbf{x}, t)]^2 - \frac{3}{2}[\mathbf{u}(\mathbf{x}, t) \cdot \mathbf{u}(\mathbf{x}, t)]\right\} \tag{3}$$

Forcing term F is used to reproduce the effect of change density due to a temperature gradient. This force modifies populations f along each lattice direction [31, 32, 44]:

$$F_\alpha(\mathbf{x}, t) = w_\alpha\{3[\mathbf{e}_\alpha - \mathbf{u}(\mathbf{x}, t)] + 9[\mathbf{e}_\alpha \cdot \mathbf{u}(\mathbf{x}, t)\mathbf{e}_\alpha]\} \cdot \mathbf{F}(\mathbf{x}, t) \tag{4}$$

Density and velocity are given by the first two moments of the distribution functions:

$$\begin{aligned} \rho(\mathbf{x}, t) &= \sum_{\alpha=0}^{N_{pop}-1} f_\alpha(\mathbf{x}, t) \\ \rho(\mathbf{x}, t)\mathbf{u}(\mathbf{x}, t) &= \sum_{\alpha=0}^{N_{pop}-1} \mathbf{e}_\alpha f_\alpha(\mathbf{x}, t) + \frac{\Delta t}{2}\mathbf{F}(\mathbf{x}, t) \end{aligned} \tag{5}$$

3. Finite volume thermal model for energy equation

It is useful to introduce now the method used to retrieve temperature evolution. Starting point is the solution of energy Eq. (6). This equation has been solved through a finite volume approach based on high-order differencing schemes, as described below.

$$\frac{\partial T(\mathbf{x}, t)}{\partial t} + \mathbf{u}(\mathbf{x}, t)\nabla T(\mathbf{x}, t) = \nabla[\chi \nabla T(\mathbf{x}, t)] \tag{6}$$

Being the velocity field known by the fluid dynamic time step, temperature becomes a passive scalar which could be directly obtained by solving Eq. (6), this is true if viscous effects are neglected. Here an explicit scheme, the simplest solution to be implemented and to exploit parallel computing, has been used. Thus, to solve Eq. (6), derivatives may be evaluated by temperature field at previous time step. In some conditions, especially in the case of conjugate heat transfer, which involves materials with thermal diffusivity far from each other, some underiterations are required with consequent penalizations in terms of computational time. Derivatives may be approximated by different schemes, the simplest one is the centred scheme which needs a stencil of only one neighbor, as reported in Eqs. (11) and (12), and results to be second-order accurate. Many other and more complicated stencils may be used, as in [45], where a stencil which somehow recalls the lattice Boltzmann one has been used. In this paper, the stencil for derivative computation has been extended to the second neighbors' belt. Obviously, this procedure may be adopted only in the inner area of the domain where all the neighbors are present. The two belt derivatives read as follows, for sake of brevity written only for one direction:

$$\left(\frac{\partial T}{\partial x}\right)_i = \frac{-T_{i+2} + 8T_{i+1} - 8T_{i-1} + T_{i-2}}{12\Delta x} + O(\Delta x)^4 \tag{7}$$

$$\left(\frac{\partial^2 T}{\partial x^2}\right)_i = \frac{-T_{i+2} + 16T_{i+1} - 30T_i + 16T_{i-1} - T_{i-2}}{12(\Delta x)^2} + O(\Delta x)^4 \tag{8}$$

Along each direction, temperature gradient and Laplacian are computed according to the values of first two neighbors. This choice requires more grid points and an overhead cost but, at the same time, it allows increasing derivatives accuracy, as per their definition. Near the walls, gradient and Laplacian terms are discretized with forward and backward difference schemes to consider only physical nodes in the computation, as reported in Eqs. (9) and (10). Of course, this implies a lack of accuracy which passes from the fourth order to the third one.

$$\left(\frac{\partial T}{\partial x}\right)_i^{BW} = \frac{2T_{i+1} + 3T_i - 6T_{i-1} + T_{i-2}}{6\Delta x} + O(\Delta x)^3 \tag{9}$$

$$\left(\frac{\partial T}{\partial x}\right)_i^{FW} = \frac{-T_{i+2} + 6T_{i+1} - 3T_i - 2T_{i-1}}{6\Delta x} + O(\Delta x)^3 \tag{10}$$

For the nodes immediately after a wall, where the two-belt stencil cannot be adopted, the one belt central scheme for gradients and for Laplacian is used, as reported in the following Eqs. (11) and (12).

$$\left(\frac{\partial T}{\partial x}\right)_i = \frac{T_{i+1} - T_{i-1}}{2\Delta x} + O(\Delta x)^2 \tag{11}$$

$$\left(\frac{\partial^2 T}{\partial x^2}\right)_i = \frac{T_{i+1} - 2T_i + T_{i-1}}{(\Delta x)^2} + O(\Delta x)^2 \tag{12}$$

Being the conjugate, heat transfers the goal of the paper, a particular attention is addressed to the definition of solid–fluid interface. A common approach used for interface wall nodes imposes the heat flux conservation. With this constraint, by assuming that the heat adducted/lost by the fluid is equal to the one lost/adducted by the solid, a fictitious wall temperature may be derived [26, 46, 47], as shown in the following Eq. (13):

$$\kappa_{\text{flu}}(T_{\text{flu}} - T_{\text{wall}}) = \kappa_{\text{sol}}(T_{\text{wall}} - T_{\text{sol}}) \Longrightarrow T_{\text{wall}} = \frac{\kappa_{\text{flu}} T_{\text{flu}} + \kappa_{\text{sol}} T_{\text{sol}}}{\kappa_{\text{flu}} + \kappa_{\text{sol}}} \tag{13}$$

where κ_{flu} and κ_{sol} represent the thermal conductivities of fluid and solid, respectively, T_{flu} and T_{sol} are the temperatures at fluid and solid nodes and T_{wall} is the wall interface temperature to be evaluated. Once all the required derivatives have been calculated, temperature can be explicitly evaluated starting from its value at the previous time step t:

$$T^{t+1} = T^t + dt\left[\chi\left(\nabla^2 T_i^t + \nabla^2 T_j^t\right) - u^{t+1}\nabla T_i^t - v^{t+1}\nabla T_j^t\right] \tag{14}$$

where i and j represent the two spatial directions and u^{t+1} and v^{t+1} are the two velocity components evaluated by the LBM. Moreover, finite time step dt has to satisfy stability condition for explicit scheme [47]:

$$dt < \frac{1}{2\max(\chi_{flu}, \chi_{sol})} \tag{15}$$

This is the reason why, in some cases, some underiterations are required to retrieve temperature evolution.

4. Model validation

In this section, different test cases have been used to validate thermal model proposed in this paper. The first test case is natural convection in a square cavity where only one fluid is present, while the second one involves the CHT and it is referred to heat exchanger in the case of pure heat conduction and in the case of flowing liquid where convection plays a role as well.

4.1. Natural convection in a square cavity

Natural convection in a square cavity is the first test case used to validate the model [21, 24, 27, 30, 31, 48–50]. In this configuration, there is a horizontal temperature gradient which causes a density gradient too. The external volume force applied to the fluid is represented by the gravitational field, thus a buoyancy force has to be considered during the simulations. The domain is a square with side of L, left side is cold and kept at temperature T_C while the right one is hot at temperature T_H. The density difference due to the temperature gradient between walls induces a fluid motion as previously mentioned. The other sides are assumed to be adiabatic. In the next Figure 2, a simple sketch of the computational domain including used boundary conditions is depicted.

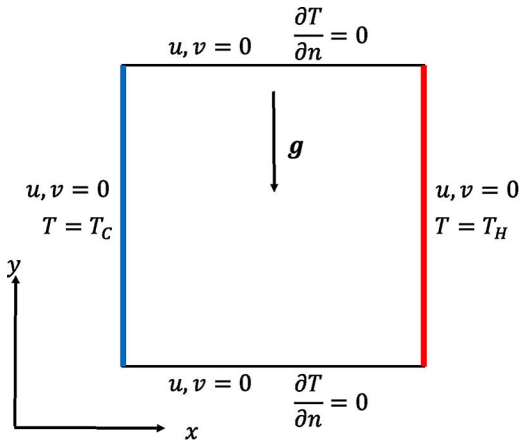

Figure 2. Schematic representation of the computational domain used for the natural convection in a square cavity.

The fluid motion is driven by the temperature difference between the walls and it is implemented through a buoyancy force modeled through the Boussinesq approximation [27, 30, 31, 49]:

$$\mathbf{F}(\mathbf{x},t) = -\rho(\mathbf{x},t)\beta\mathbf{g}[T(\mathbf{x},t) - T_0] \tag{16}$$

where:

- $\rho(x, t)$ is the local density;
- β is the thermal expansion coefficient;
- $\mathbf{g}$ is the gravitational acceleration;
- $T_0 = \frac{T_C+T_H}{2}$ is the mean temperature.

In the range of analyzed Rayleigh numbers, the fluid properties may be considered to be constant. More specifically, the problem is governed by Rayleigh and Prandtl numbers, which are reported in the following Eqs. (17) and (18):

$$\mathrm{Ra} = \frac{\beta|\mathbf{g}|\Delta TL^3}{\nu\chi} \tag{17}$$

$$\mathrm{Pr} = \frac{\nu}{\chi} \tag{18}$$

where ΔT is the temperature difference $T_H - T_C$. As well known, the LBM is valid under weakly compressible conditions, thus, to limit the maximum velocity reached, a characteristic speed U_c, function of simulation parameters, can be defined:

$$U_c = \sqrt{\beta|\mathbf{g}|\Delta TL} \tag{19}$$

By limiting this parameter, it is possible to evaluate the proper forcing magnitude for the considered operating conditions. As a consequence, the forcing term depends on U_c and grid size when wall temperatures are fixed:

$$\beta|\mathbf{g}| = \frac{U_c^2}{\Delta TL} \tag{20}$$

Once Rayleigh and Prandtl numbers are defined, U_c can be chosen and the main LBM parameters may be consequently evaluated:

$$\nu = \sqrt{\frac{\mathrm{Pr}}{\mathrm{Ra}}}U_cL \Longrightarrow \tau_f = 3\nu + \frac{1}{2} \tag{21}$$

$$\chi = \frac{U_cL}{\sqrt{\mathrm{RaPr}}} \tag{22}$$

Next Table 1 shows setting parameters for different Rayleigh numbers, with keeping constant Prandtl number equal to 0.71:

4.1.1. Results

In this subsection, the results obtained for different Rayleigh numbers are compared with reference data available in the literature [21, 24, 27, 30, 31, 48, 49]. Results are compared in terms of:

Table 1. Setting parameters for natural convection in a square box analysis.

Ra	10^3	10^4	10^5	10^6
Grid size	100 × 100	150 × 150	200 × 200	200 × 200
U_c	0.01	0.02	0.1	0.1
ν	0.0266	0.0253	0.0533	0.0169
χ	0.0375	0.0356	0.0751	0.0237
τ_f	0.580	0.576	0.660	0.550

Table 2. Comparison between results and the reference data for different Rayleigh numbers.

	$Ra = 10^3$		$Ra = 10^4$	
	FVM	Ref.	FVM	Ref.
u_{max}	3.648	3.647/4.077	16.183	16.154/16.262
y_{max}	0.815	0.806/0.813	0.823	0.818/0.823
v_{max}	3.695	3.697/4.130	19.620	19.601/19.717
x_{max}	0.175	0.178/0.181	0.117	0.118/0.120
Nu_{ave}	1.1176	1.114/1.118	2.2441	2.229/2.246
	$Ra = 10^5$		$Ra = 10^6$	
	FVM	Ref.	FVM	Ref.
u_{max}	34.709	34.508/35.172	64.7624	63.456/64.992
y_{max}	0.853	0.853/0.859	0.848	0.848/0.859
v_{max}	68.621	68.538/68.746	220.393	219.360/220.765
x_{max}	0.0675	0.065/0.067	0.0375	0.036/0.039
Nu_{ave}	4.518	4.489/4.526	8.803	8.750/8.825

- maximum horizontal velocity u_{max} and its position y_{max} along vertical mid-line;
- maximum vertical velocity v_{max} and its position x_{max} along horizontal mid-line;
- surfaced-averaged Nusselt number at the hot wall Nu_{ave};

Velocities are normalized using the reference velocity χ/L, while the coordinate is normalized by the characteristic length L. Assuming $\Delta T = T_H - T_C$ and n, the normal vector to the surface, the local Nusselt number is [27, 31, 48, 49]:

$$Nu_{loc} = \frac{L}{\Delta T}\frac{\partial T}{\partial n} \tag{23}$$

Local Nusselt number can be integrated along the whole hot wall length to compute the average Nusselt number.

$$Nu_{ave} = \frac{1}{L}\int_0^L Nu_{loc} \cdot ds = \frac{1}{\Delta T}\int_0^L \frac{\partial T}{\partial n} \cdot ds \tag{24}$$

In Table 2 obtained results are compared with the available literature data for all the Rayleigh numbers analyzed.

From Table 2, it may be highlighted how the proposed method properly fits reference data available in the literature. These results are also depicted in the next Figure 3 where the evaluated Nu number is reported as a function of the expected one.

The influence of Rayleigh number variation on velocity and temperature fields is briefly summarized in Figure 4. From this figure, it may be easily observed how the Rayleigh number tends

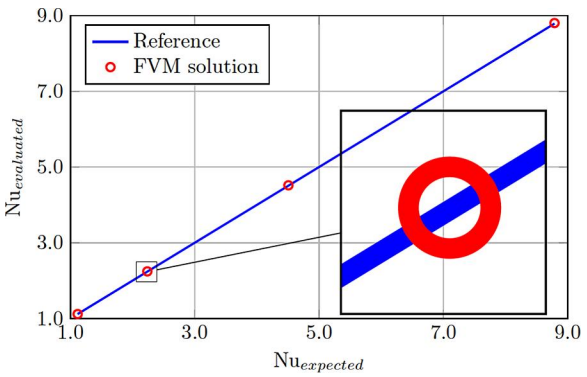

Figure 3. Comparison between expected and evaluated Nusselt number. The blue line represents the expected values, while the colored markers represent the LBM-FVM results.

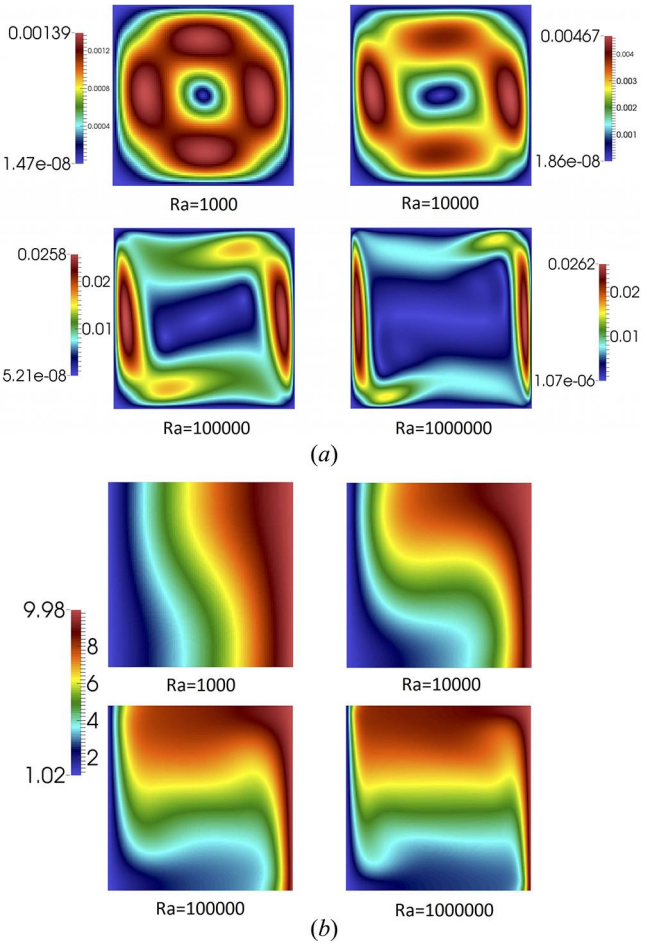

Figure 4. Velocity and Temperature contours for different Rayleigh numbers. (a) Velocity and (b) Temperature.

to deviate both velocity and temperature fields and how the temperature gradient is aligned along the horizontal direction, while the gravity force, and then the buoyancy term, here considered, are aligned along the vertical direction.

4.2. Counterflow heat exchanger

In the previous Section 4.1, results for natural convection have been presented for the proposed solver based on high-order derivatives. This preliminary example is related to a single phase/material problem, where only one kind of fluid is present and conjugate heat transfer is not considered. In this section, CHT, where there is an interface between two different phases, is analysed with focusing on a counterflow heat exchanger in two operating conditions. In the first one, the fluid is stagnant into channels and top and bottom walls are at constant temperature (pure conduction test case). In the second example, the fluid is driven by a pressure drop and inlet temperature is imposed on the left and on the right side of the heat exchanger [26], while north and bottom walls are adiabatic. It may be trivially pointed out that the latter test case is a mixed convection/conduction heat transfer problem. For both heat transfer problems, the computational domain is made up of two parallel channels separated by a solid zone. Channel length L is 10 times the height h ($L = 10h$) to have a developed flow in the channels. Other operating parameters are schematically represented in the next Figure 5.

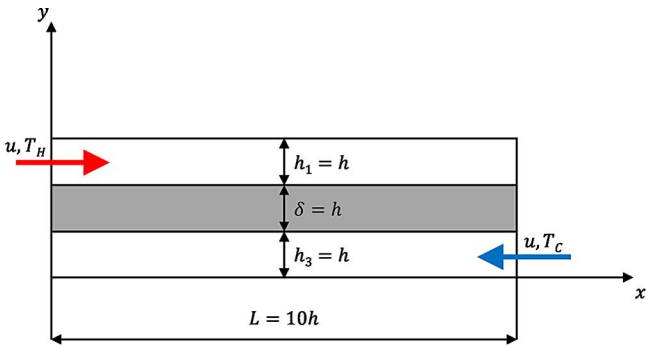

Figure 5. Representation of the computational domain for the counterflow heat exchanger. The darker gray layer represents the thin metal plate between the two fluid channels.

4.2.1. Pure conduction heat transfer

A first check of the model is performed with a pure heat conduction problem where the analytical solution is known. The computational domain is the one represented in Figure 5, but with applying different boundary conditions (BCs). More specifically, all fluid dynamics BCs are solid walls (u, $v = 0$), while the thermal BCs are imposed temperature for north and south walls (respectively, hot and cold T_H and T_C), and adiabatic walls for left and right sides. With these constraints, the solution is one-dimensional and the heat flux can be exactly evaluated starting from imposed values. The analytical expression for the heat flux is reported in the following equation:

$$Q = \frac{T_H - T_C}{\left(\frac{2h}{\kappa_{\text{flu}}} + \frac{\delta}{\kappa_{\text{sol}}}\right)} = 22727.2727 \text{ W/m}^2 \tag{25}$$

where:

- $T_H = 800$ K and $T_C = 300$K;
- $h = 0.1$ m;
- $\delta = 0.1$ m;
- $\kappa_{\text{flu}} = 10.0$ W/mK and $\kappa_{\text{sol}} = 50.0$ W/mK.

To better represent results the nondimensional temperature $\widetilde{T}$ can be considered, according to the following definition:

$$\widetilde{T} = \frac{T - T_C}{T_H - T_C} \tag{26}$$

As per its definition, $\widetilde{T}$ may vary in the range 0–1. Figure 6 highlights the very good matching between the expected results and those obtained from simulations, where the nondimensional coordinate has been obtained by dividing the vertical coordinate y for the total height, $\tilde{y} = \frac{y}{2h+\delta}$.

Once having validated a steady-state pure conduction problem, as reported in Figure 6, the next subsection reports analysis results in the case of conduction/convection heat transfer test case.

4.2.2. Mixed convection/conduction heat transfer

In this section, results obtained with the proposed coupled method are compared with the ones presented in [26]. As already anticipated, in this condition, the fluid is not at rest any more and it has inlet velocity different from zero, which leads to the contemporary presence of two heat exchange mechanisms, conduction, and convection. To compare results with available literature data, parameters reported in Table 3 are used in simulation setup. FVM solver does not need to make

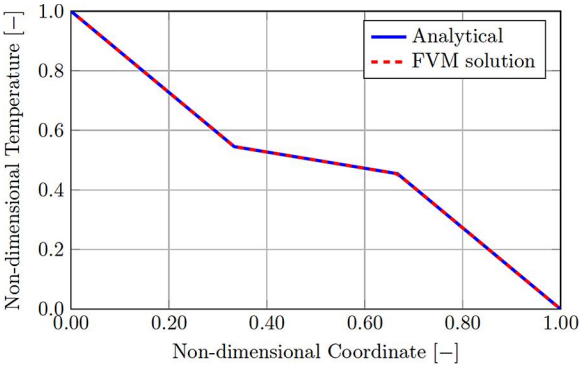

Figure 6. Nondimensional temperature in pure heat conduction. The solid blue line represents the analytical solution perfectly overlapped with the red-colored dashed line representative of the proposed method.

any assumption on thermal capacity, which is, on the other hand, one of the weak points commonly highlighted for thermal LBM, where the same thermal capacity has to be assumed for both solid and fluid because of requirement of temperature and heat flux continuities at interface wall [22].

When the steady-state solution is reached, comparison is performed through analyzing temperature behavior along a vertical line corresponding to $x = L/2$, as reported in Figure 7.

As can be seen from Figure 7, there is a perfect agreement on the steady-state solution between the proposed method and the literature data. Once having performed the validation in a mixed conduction/convection test case, it is possible to deal with the test case proposed and discussed in the following section, the CHT in a counterflow heat exchanger with a porous insert.

Table 3. Properties for the counterflow heat exchanger.

	h_1	δ	h_3
ρ[kg/m^3]	1000	8000	1000
c_p[J/(kgK)]	25	500	25
κ[W/(mK)]	10	50	10
ν[m^2/s]	0.00015	–	0.00015
Pr	0.375	–	0.375
L[m]	0.1	0.1	0.1
Inlet temperature (T_H/T_C) [K]	800	–	300
Inlet velocity (u) [m/s]	0.2	–	0.1

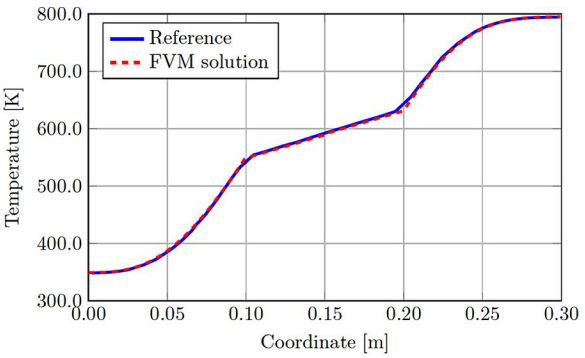

Figure 7. Temperature profile along vertical section and comparison with available literature data.

5. Heat exchanger with porous medium

As already mentioned, porous media are gaining a relevant role in many engineering applications due to their thermomechanical properties. In this section, the capabilities of the proposed thermal method to deal with complex geometries are highlighted. Thus, thermal behavior of a counterflow heat exchanger with an insert of porous material, so to improve thermal transfer mechanisms, is analyzed. Heat exchanger dimensions are the same presented in previous section 4.2, but into upper and lower channels, an insert made of open-cell metal foam is considered to improve heat exchange process. As one can be easily figure out, CHT in such an apparatus is quite tricky due to the intrinsic difficulty in dealing with complex boundaries. Nevertheless, the proposed method, based on the coupling between LBM and FVM, allows reconstructing both fluid and thermal fields in a satisfactory manner.

5.1. Porous media modeling

Before presenting thermal analysis, it is important to define how the two dimensional porous medium has been modeled. In this work, the porous medium generation starts from the random packing sphere approach proposed by Al-Raoush and Alsaleh [18] and already analyzed by the authors in [9]. In this application, a similar model for random packing circles into an initially filled metal box is used; the area inside every circle represents the vacuum where air can pass through. Porosity ε equal to 95% and inlet Reynolds number, evaluated as $\mathrm{Re} = \frac{uh}{\nu}$, in the range 50–150 are main simulation parameters. In the following figure, the computational domain is reported to highlight the metal foam present into heat exchanger channels.

With referring to Figure 8, it can be highlighted how the main proportions of the heat exchangers are the same presented in Figure 5, except for the presence of porous medium. To stabilize inlet and outlet boundary conditions, the porous insert does not cover the whole channel length. In this application, an aluminium metal foam has been considered, while fluid is considered to be air. Simulation parameters are briefly reported in the following Table 4.

5.2. Results

To be able to evaluate the effect of porous medium on heat exchange process, a preliminary set of simulations has been done where the fluid channels are empty and thus air can flow through without encountering obstacles. This is the standard counterflow heat exchanger configuration and simulations have performed for three different values of Reynolds number (50, 100, and 150), the ones which will be analyzed when the porous medium is present as well. In the following figures, temperature distributions for the three considered Re are presented, both for standard and porous heat exchangers. Moreover, to better quantify, the advantages of such a material for heat exchange process, the log mean temperature difference (LMDT) is evaluated for all the conditions analyzed. To evaluate this quantity, the mixing cup temperature [51], is used to determine

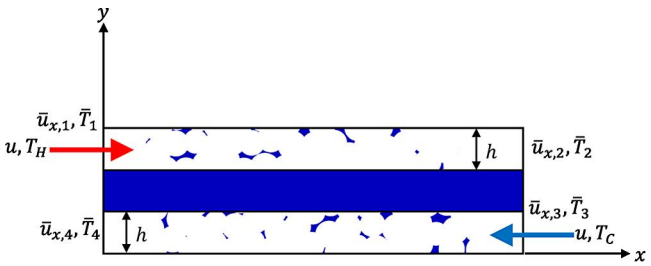

Figure 8. Counterflow heat exchanger with porous medium. The dark blue areas represent metal zones into air volume. The different sections used for result comparison are highlighted in the outer area.

Table 4. Properties for the counterflow heat exchanger with porous medium.

	Air	Aluminium
ρ[kg/m^3]	1.184	2700
c_p[J/(kgK)]	1007	900
κ[W/(mK)]	0.02551	150
ν[m^2/s]	0.000015617	–
Pr	0.72	–
Re	50–150	–
Inlet Temperature (T_H/T_C) [K]	800/300	–

the mean temperatures at inlet/outlet sections. More specifically, this average temperature may be evaluated as follows:

$$\overline{T} = \frac{1}{h\bar{u}_x}\int_h u_x T dy \tag{27}$$

where h represents the height of the flow channel, $\bar{u}_x$ the mean velocity along the x direction (same as of ΔT), u_x and T are the local horizontal velocity component and temperature at the specific y. More in detail, four different average temperatures are needed to evaluate the LMDT, with referring to Figure 8 they are named $\overline{T}_1, \overline{T}_2, \overline{T}_3$, and $\overline{T}_4$ and depend on four average velocities $u_{x,1}$, $u_{x,2}$, $u_{x,3}$, and $u_{x,4}$ integrated along the channel height h. Thus, the LMDT may be evaluated as follows:

$$\mathrm{LMDT} = \frac{\left(\overline{T}_2 - \overline{T}_1\right) - \left(\overline{T}_3 - \overline{T}_4\right)}{\log\left(\overline{T}_2 - \overline{T}_1\right) - \log\left(\overline{T}_3 - \overline{T}_4\right)} \tag{28}$$

Results for both empty channels and porous ones in terms of LMDT are summarized in the following Table 5.

It is worth nothing that the porous medium allows increasing the heat exchange which corresponds to lower values of LMDT for all the Re numbers considered with an increased amount of heat exchanged. More specifically, the heat flux increases about 10% for Re = 50 and about 40% for Re = 150 when porous insert is considered. Another comparison may be done with analyzing temperature trend along two horizontal lines which corresponds to two different heights $y = 0$ and $y = 3h$, namely, the bottom and the upper walls. In the next Figure 9 empty markers represent the empty configuration, while the filled ones are referred to porous channels.

Again, Figure 9 highlights how the presence of porous insert allows exploiting heat transfer mechanisms with temperature gradients steeper than the empty channel configuration. This would allow reducing heat exchanger length if the target is to reach a specific temperature difference. On the other hand, once having fixed channel length, porous insert allows increasing the heat exchanged with evident benefits in terms of efficiencies. Finally, results are compared by looking at temperature maps depicted in Figure 10, only for one Reynolds number, Re = 150.

Figure 10 clearly shows how the presence of open-cell metal foam generates turbulence which exploits mixing and, as a consequence, hardly modifies temperature evolution along the channels where the air passes through.

Table 5. LMDT and heat flux comparison for empty channels and porous ones as a function of inlet Re.

	Empty		Porous	
	LMDT	$\dot{Q}$	LMDT	$\dot{Q}$
Re = 50	353	84596.41	342	92898.91
Re = 100	397	118631.67	373	141388.41
Re = 150	415	146957.91	399	200583.58

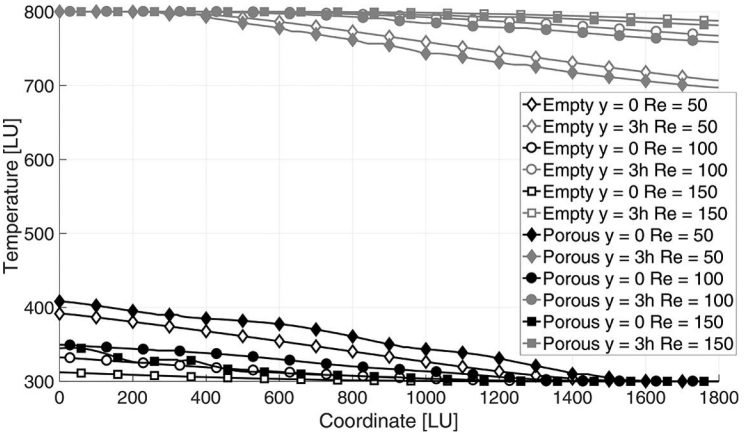

Figure 9. Temperature evolution along channels for both empty and porous heat exchangers. Black lines represent coordinate $y = 0$, gray ones $y = 3h$; empty markers are referred to empty heat exchanger, filled ones to the porous heat exchanger; diamonds are for Re = 50, circles for Re = 100, and squares for Re = 150.

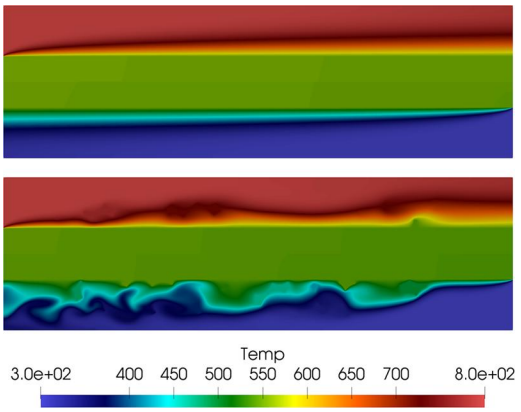

Figure 10. Temperature maps for both empty (upper) and porous (lower) heat exchangers.

6. Conclusion

In this paper, a coupled method LBM-VFM for conjugate heat transfer problems has been presented. This is based on a standard D_2Q_9 LB framework coupled with high-order differencing schemes for energy equation solution. The presented method has been first validated with the well-known literature test cases with good results, and then, it has been analyzed a more complex test case. More specifically, the flow through a counterflow heat exchanger has been studied with and without a porous medium insert. The porous medium, representative of an open-cell metal foam, has been obtained by a random packing sphere approach. Three different inlet Reynolds numbers have been considered to fully validate the proposed method. Results have shown a strong impact of porous medium insert in heat exchange properties. A valuable increment of heat flux has been measured for all the studied configurations when metal foam has been placed into channels with the possibility to reduce heat exchanger length if the heat flux is the target. The coupled method has shown excellent performance while dealing with conjugate heat transfer across complex boundary conditions, with the possibility to extend it to three-dimensional framework for more complex test cases.

Funding

The numerical simulations were performed on *Zeus* HPC facility, at the University of Naples "Parthenope"; *Zeus* HPC has been realized through the Italian Government Grant PAC01_00119 *MITO - Informazioni Multimediali per Oggetti Territoriali*, with Prof. Elio Jannelli as the Scientific Responsible.

ORCID

D. Chiappini http://orcid.org/0000-0002-5316-4434

References

[1] A. Bhattacharya and R. L. Mahajan, "Finned metal foam heat sinks for electronics cooling in forced convection," *J. Electron. Packag.*, vol. 124, no. 3, pp. 155–163, 2002. DOI: 10.1115/1.1464877.
[2] S. Mahjoob and K. Vafai, "A synthesis of fluid and thermal transport models for metal foam heat exchangers," *Int. J. Heat Mass Transfer*, vol. 51, pp. 3701–3711, 2008. DOI: 10.1016/j.ijheatmasstransfer.2007.12.012.
[3] S. Succi, *The Lattice Boltzmann Equation for Fluid Dynamics and Beyond*. Oxford: Clarendon Press, 2001.
[4] S. Chen and G. D. Doolen, "Lattice Boltzmann method for fluid flows," *Ann. Rev. Fluid Mech.*, vol. 30, no. 1, pp. 329–364, 1998. DOI: 10.1146/annurev.fluid.30.1.329.
[5] C. K. Aidun and J. R. Clausen, "Lattice-Boltzmann method for complex flows," *Ann. Rev. Fluid Mech.*, vol. 42, pp. 439–472, 2010. DOI: 10.1146/annurev-fluid-121108-145519.
[6] J. Hao and L. Zhu, "A lattice Boltzmann based implicit immersed boundary method for fluid-structure interaction," *Comput. Math. Appl.*, vol. 59, no. 1, pp. 185–193, 2010. DOI: 10.1016/j.camwa.2009.06.055.
[7] D. Beugre, S. Calvo, G. Dethier, M. Crine, D. Toye, P. Marchot, et al., "Lattice Boltzmann 3D flow simulations on a metallic foam," *J. Comput. Appl. Math.*, vol. 234, pp. 2128–2134, 2010. DOI: 10.1016/j.cam.2009.08.100.
[8] A. Montessori, G. Falcucci, P. Prestininzi, M. La Rocca, and S. Succi, "Regularized lattice Bhatnagar–Gross–Krook model for two- and three-dimensional cavity flow simulations," *Phys. Rev. E*, vol. 89, pp. 1–8, 2014. DOI: 10.1103/PhysRevE.89.053317.
[9] D. Chiappini, G. Bella, A. Festuccia, and A. Simoncini, "Direct numerical simulation of an open-cell metallic foam through lattice Boltzmann method," *Commun. Comput. Phys.*, vol. 18, no. 3, pp. 707–722, 2015. DOI: 10.4208/cicp.191114.270315a.
[10] G. Di Ilio, D. Chiappini, S. Ubertini, G. Bella, and S. Succi, "Hybrid lattice Boltzmann method on overlapping grids," *Phys. Rev. E*, vol. 95, no. 1, p. 013309, 2017. DOI: 10.1103/PhysRevE.95.013309.
[11] G. Falcucci, G. Bella, G. Chiatti, S. Chibbaro, M. Sbragaglia, S. Succi, et al., "Lattice Boltzmann models with mid-range interactions," *Commun. Comput. Phys.*, vol. 2, no. 6, pp. 1071–1084, 2007.
[12] G. Bella, D. Chiappini, and S. Ubertini, "Modeling liquid break-up through a kinetic approach," *SAE Int. J. Eng.*, vol. 2, no. 3, pp. 390–399, 2010. DOI: 10.4271/2009-24-0023.
[13] G. Falcucci, S. Ubertini, D. Chiappini, and S. Succi, "Modern lattice Boltzmann methods for multiphase microflows," *IMA J. Appl. Math.*, vol. 76, no. 5, pp. 712–725, 2011. DOI: 10.1093/imamat/hxr014.
[14] M. Ashrafizaadeh and H. Bakhshaei, "A comparison of non-Newtonian models for lattice Boltzmann blood flow simulations," *Comput. Math. Appl.*, vol. 58, no. 5, pp. 1045–1054, 2009. DOI: 10.1016/j.camwa.2009.02.021.
[15] G. Di Ilio, D. Chiappini, and G. Bella, "A comparison of numerical methods for non-Newtonian fluid flows in a sudden expansion," *Int. J. Modern Phys. C*, vol. 27, no. 11, p. 1650139, 2016. DOI: 10.1142/S0129183116501394.
[16] A. Montessori, P. Prestininzi, M. La Rocca, G. Falcucci, S. Succi, E. Kaxiras, et al., "Effects of Knudsen diffusivity on the effective reactivity of nanoporous catalyst media," *J. Comput. Sci.*, vol. 17, pp. 377–383, 2015. DOI: 10.1016/j.jocs.2016.04.006.
[17] V. K. Krastev, G. Amati, E. Jannelli, and G. Falcucci, "Direct numerical simulation of SCR reactors through kinetic approach," in: SAE Technical Paper - 2016-01-0963, SAE International, Detroit, SAE Technical Paper— 2016-01-0963, 2016. DOI: 10.4271/2016-01-0963.
[18] R. Al-Raoush and M. Alsaleh, "Simulation of random packing of polydisperse particles," *Powder Technol.*, vol. 176, no. 1, pp. 47–55, 2007. DOI: 10.1016/j.powtec.2007.02.007.
[19] A. D'Orazio, M. Corcione, and G. P. Celata, "Application to natural convection enclosed flows of a lattice Boltzmann BGK model coupled with a general purpose thermal boundary condition," *Int. J. Therm. Sci.*, vol. 43, no. 6, pp. 575–586, 2004. DOI: 10.1016/j.ijthermalsci.2003.11.002.
[20] A. D'Orazio and S. Succi, "Simulating two-dimensional thermal channel flows by means of a lattice Boltzmann method with new boundary conditions," *Future Gener. Comput. Syst.*, vol. 20, no. 6, pp. 935–944, 2004. DOI: 10.1016/j.future.2003.12.005.
[21] H. N. Dixit and V. Babu, "Simulation of high Rayleigh number natural convection in a square cavity using the lattice Boltzmann method," *Int. J. Heat Mass Transfer*, vol. 49, nos. 3–4, pp. 727–739, 2006. DOI: 10.1016/j.ijheatmasstransfer.2005.07.046.

[22] M. Wang, J. He, J. Yu, and N. Pan, "Lattice Boltzmann modeling of the effective thermal conductivity for fibrous materials," *Int. J. Therm. Sci.*, vol. 46, no. 9, pp. 848–855, 2007. DOI: 10.1016/j.ijthermalsci.2006.11.006.
[23] S. Gokaltun and G. S. Dulikravich, "Lattice Boltzmann computations of incompressible laminar flow and heat transfer in a constricted channel," *Comput. Math. Appl.*, vol. 59, no. 7, pp. 2431–2441, 2010. DOI: 10.1016/j.camwa.2009.08.045.
[24] C.-H. Liu, K.-H. Lin, H.-C. Mai, and C.-A. Lin, "Thermal boundary conditions for thermal lattice Boltzmann simulations," *Computers &. Math. Appl.*, vol. 59, no. 7, pp. 2178–2193, 2010. DOI: 10.1016/j.camwa.2009.08.043.
[25] Q. Liao and T.-C. Jen, *Application of Lattice Boltzmann Method in Fluid Flow and Heat Transfer*. London, UK: INTECH Open Access Publisher, 2011.
[26] X. Chen and P. Han, "A note on the solution of conjugate heat transfer problems using SIMPLE-like algorithms," *Int. J. Heat Fluid Flow*, vol. 21, no. 4, pp. 463–467, 2000. DOI: 10.1016/S0142-727X(00)00028-X.
[27] Y. Peng, C. Shu, and Y. T. Chew, "Simplified thermal lattice Boltzmann model for incompressible thermal flows," *Phys. Rev. E*, vol. 68, no. 2, pp. 1–8, 2003. DOI: 10.1103/PhysRevE.68.026701.
[28] F. Kuznik and G. Rusaouen, "Numerical prediction of natural convection occurring in building components: A double-population lattice boltzmann method," *Numer. Heat Transfer, Part A: Appl.*, vol. 52, no. 4, pp. 315–335, 2007. DOI: 10.1080/00397910601149959.
[29] J. Cai and X. Huai, "Study on fluid-solid coupling heat transfer in fractal porous medium by lattice Boltzmann method," *Appl. Therm. Eng.*, vol. 30, nos. 6–7, pp. 715–723, 2010. DOI: 10.1016/j.applthermaleng.2009.12.001.
[30] H.-C. Mai, K.-H. Lin, C.-H. Yang, and C.-A. Lin, "A thermal lattice Boltzmann model for flows with viscous heat dissipation," *Comput. Model. Engineering & Sci.*, vol. 61, no. 1, pp. 45–63, 2010.
[31] A. A. Mohamad and A. Kuzmin, "A critical evaluation of force term in lattice Boltzmann method, natural convection problem," *Int. J. Heat Mass Transfer*, vol. 53, nos. 5–6, pp. 990–996, 2010. DOI: 10.1016/j.ijheatmasstransfer.2009.11.014.
[32] R. Khazaeli, S. Mortazavi, and M. Ashrafizaadeh, "Application of a ghost fluid approach for a thermal lattice Boltzmann method," *J. Comput. Phys.*, vol. 250, pp. 126–140, 2013. DOI: 10.1016/j.jcp.2013.04.044.
[33] A. Tarokh, A. A. Mohamad, and L. Jiang, "Simulation of conjugate heat transfer using the lattice Boltzmann method," *Numer. Heat Transfer, Part A: Appl.*, vol. 63, no. 3, pp. 159–178, 2013. DOI: 10.1080/10407782.2012.725009.
[34] C. Demuth, M. A. Mendes, S. Ray, and D. Trimis, "Performance of thermal lattice Boltzmann and finite volume methods for the solution of heat conduction equation in 2D and 3D composite media with inclined and curved interfaces," *Int. J. Heat Mass Transfer*, vol. 77, pp. 979–994, 2014. DOI: 10.1016/j.ijheatmasstransfer.2014.05.051.
[35] H. S. Amir and K. Mohammad, "Numerical investigation of nanofluid flow and conjugated heat transfer in a micro-heat-exchanger using the lattice boltzmann method," *Numer. Heat Transfer, Part A: Appl.*, vol. 70, no. 12, pp. 1390–1401, 2016. DOI: 10.1080/10407782.2016.1244394.
[36] S. C. Mishra, S. Panigrahy, and V. J. Ghatage, "Analysis of combined mode heat transfer in a porous medium using the lattice boltzmann method," *Numer. Heat Transfer, Part A: Appl.*, vol. 69, no. 10, pp. 1092–1105, 2016. DOI: 10.1080/10407782.2015.1125711.
[37] S. Biswas, P. Sharma, B. Mondal, and G. Biswas, "Analysis of mixed convective heat transfer in a ribbed channel using the lattice boltzmann method," *Numer. Heat Transfer, Part A: Appl.*, vol. 68, no. 1, pp. 75–98, 2015. DOI: 10.1080/10407782.2014.965095.
[38] G. Imani, M. Maerefat, and K. Hooman, "Lattice boltzmann simulation of conjugate heat transfer from multiple heated obstacles mounted in a walled parallel plate channel," *Numer. Heat Transfer, Part A: Appl.*, vol. 62, no. 10, pp. 798–821, 2012. DOI: 10.1080/10407782.2012.709442.
[39] M. A. Moussaoui, M. Jami, A. Mezrhab, and H. Naji, "Lattice boltzmann simulation of convective heat transfer from heated blocks in a horizontal channel," *Numer. Heat Transfer, Part A: Appl.*, vol. 56, no. 5, pp. 422–443, 2009. DOI: 10.1080/10407780903244338.
[40] D. Chiappini, "Numerical simulation of natural convection in open-cells metal foams," *Int. J. Heat Mass Transfer*, vol. 117, pp. 527–537, 2018. DOI: 10.1016/j.ijheatmasstransfer.2017.10.022.
[41] L. Li, C. Chen, R. Mei, and J. F. Klausner, "Conjugate heat and mass transfer in the lattice Boltzmann equation method," *Phys. Rev. E*, vol. 89, 043308–1–21. DOI: 10.1103/PhysRevE.89.043308.
[42] G. Pareschi, N. Frapolli, S. S. Chikatamarla, and I. V. Karlin, "Conjugate heat transfer with the entropic lattice Boltzmann method," *Phys. Rev. E*, vol. 94, no. 1, pp. 013305, 2016. DOI: 10.1103/PhysRevE.94.013305.
[43] K. Xu and X. He, "Lattice Boltzmann method and gas-kinetic BGK scheme in the low-Mach number viscous flow simulations," *J. Comput. Phys.*, vol. 190, no. 190, pp. 100–117, 2003. DOI: 10.1016/S0021-9991(03)00255-9.
[44] Z. Guo, C. Zheng, and B. Shi, "Discrete lattice effects on the forcing term in the lattice Boltzmann method," *Phys. Rev. E—Stat., Nonlinear, Soft Matter Phys.*, vol. 65, no. 4, 046308–1–6. DOI: 10.1103/PhysRevE.65.046308.
[45] S. Bettaibi, F. Kuznik, E. Sediki, and S. Succi, "Lattice Boltzmann simulation of mixed convection heat transfer in a driven cavity with non-uniform heating of the bottom wall," *Commun. Theor. Phys.*, vol. 63, no. 1, pp. 91–100, 2015. DOI: 10.1016/j.physleta.2014.06.032.
[46] A. A. Mohamad, Q. W. Tao, Y. L. He, and S. Bawazeer, "Treatment of transport at the interface between multilayers via the lattice Boltzmann method," *Numer. Heat Transfer, Part B: Fundam.*, vol. 67, no. 2, pp. 124–134, 2014. DOI: 10.1080/10407790.2014.949563.

[47] S. Patankar, *Numerical Heat Transfer and Fluid Flow*. New York: Hemisphere Publishing Corporation, 1980.
[48] C. Shu, Y. Peng, and Y. T. Chew, "Simulation of natural nonvection in a square cavity By Taylor series expansion- and least squares-based lattice Boltzmann method," *Int. J. Modern Phys. C*, vol. 13, no. 10, pp. 1399–1414, 2002. DOI: 10.1142/S0129183102003966.
[49] Y. Peng, C. Shu, and Y. T. Chew, "A 3D incompressible thermal lattice Boltzmann model and its application to simulate natural convection in a cubic cavity," *J. Comput. Phys.*, vol. 193, no. 1, pp. 260–274, 2004. DOI: 10.1016/j.jcp.2003.08.008.
[50] T. Zhang and D. Che, "Lattice boltzmann simulation of natural convection in an inclined square cavity with spatial temperature variation," *Numer. Heat Transfer, Part A: Appl.*, vol. 66, no. 6, pp. 712–732, 2014. DOI: 10.1080/10407782.2014.894408.
[51] W. M. Rohsenow and J. R. Hartnett, *Handook of Heat Transfer*. New York, NY: McGraw-Hill, 1998.